Advanced Materials

ADVANCED MATERIALS
www.advmat.de

RESEARCH ARTICLE OPEN ACCESS

Harnessing Chain Mobility via Protonation for Tough and Isotropic Hydrogel

Pengju Shi[1] | Muqing Si[1] | Zishang Lin[1] | Qian Mao[2] | Sidi Duan[1] | Zixiao Liu[1] | Wen Hong[1] | Mason Possinger[1] | Yichen Yan[1] | Chi Chen[1] | Ping He[1] | Xiaobing Zuo[3] | Hua Zhou[3] | Adri van Duin[2] | Ximin He[1]

[1]Department of Material Science and Engineering, University of California, Los Angeles, California, USA | [2]Department of Mechanical Engineering, Pennsylvania State University, State College, Pennsylvania, USA | [3]X-Ray Science Division, Argonne National Laboratory, Lemont, Illinois, USA

Correspondence: Adri van Duin (acv13@psu.edu) | Ximin He (ximinhe@ucla.edu)

Received: 4 September 2025 | **Revised:** 19 January 2026 | **Accepted:** 5 February 2026

Keywords: acidification | hydrogen bonding | poly(vinyl alcohol) | salting out | tough hydrogel

ABSTRACT

Fabricating hydrogels with isotropically high tensile strength, stretchability, and toughness is crucial for applications in tissue engineering, stretchable bioelectronics and soft robots. However, many toughening strategies, including mechanical training, directional freezing, and solvent exchange, often induce anisotropy or fail to enhance all these metrics simultaneously. Herein, we report a strategy to fabricate ultra-tough, isotropic poly(vinyl alcohol) (PVA) hydrogels by synergistically modulating polymer chain mobility and physical crosslinking through sequential acidification, freeze-thawing, and salting-out. Acidification protonates the hydroxyl groups, suppressing premature interchain hydrogen bonding and promoting network homogenization. Subsequent salting-out deprotonates the hydroxyl groups to strengthen the interpolymer hydrogen bonds, forming crystalline domains that act as strong, reversible physical crosslinks. The resulting hydrogel achieves a high tensile strength of 29.5 MPa, stretchability of 2683%, and record-high toughness of 424 MJ m^{-3} among isotropic hydrogels, even surpassing most anisotropic hydrogels in their reinforced direction. This strategy offers a generalizable platform for engineering tough, isotropic hydrogels with broad potential across bioengineering, additive manufacturing, and soft robotics.

1 | Introduction

Hydrogels are 3D crosslinked networks swollen with water, offering high biocompatibility and tunable mechanical properties, making them attractive for a wide range of applications, including tissue engineering [1], drug delivery [2], and soft robotics [3]. In particular, the structural and compositional similarity of hydrogels to native biological tissues, such as high water content and molecular-level flexibility, make them promising materials for tissue scaffolds and stretchable bioelectronics [4–6]. However, the real-world application of conventional hydrogels is often impeded by its poor mechanical properties, including low tensile strength, stretchability, fatigue resistance, and toughness.

To address these limitations, various toughening strategies have been developed recently, including double network [7], mechanical training [8], doping with nanofillers [9, 10], etc. Many of these strategies have demonstrated substantial improvement in toughness, enabling hydrogels to sustain large deformations. Nevertheless, many strategies reported to achieve ultra-high toughness (>100 MJ m^{-3}) inherently result in anisotropic mechanical properties, where the enhancement is confined to a preferred direction. For instance, methods involving mechanical training

Pengju Shi, Muqing Si, Zishang Lin, and Qian Mao contributed equally to this work.

[8], stretch-induced chain alignment [11, 12], or directional freezing [13] promote polymer chain alignment that concentrates load-bearing capability along the alignment axis. While advantageous in specific scenarios, such anisotropy becomes a critical disadvantage in applications where the hydrogel is subjected to complex, multiaxial mechanical loading, such as in wearable bioelectronics and flexible batteries [14, 15]. Specifically, anisotropic hydrogels strengthened by aligned structures are prone to fail under off-axis loads often due to interchain debonding and lack of crack-arresting mechanisms. In contrast, isotropic hydrogels provide uniform mechanical performance in all directions, supporting structural integrity under dynamic, multidirectional stress. For example, in stretchable bioelectronics or soft energy storage devices, where hydrogels must maintain conductivity and adhesion under multimodal loads like bending, twisting, and stretching, isotropic toughness is essential for their practical operation. Moreover, isotropic hydrogels such as injectable hyaluronic acid or gelatin-based networks provide uniform mechanical support and facilitate homogeneous cell growth, making them valuable as scaffolds for cartilage and bone tissue engineering where consistent mechanical cues and nutrient transport in all directions are required [16]. To toughen the hydrogel while maintaining its mechanical isotropy, candidate strategies include double-network architectures, where a brittle sacrificial network dissipates energy while a ductile network maintains integrity [7]; nanocomposite hydrogels, in which embedded nanoparticles or fillers enhance strength and toughness [9]; and slide-ring and other topological networks that promote reversible mobility under strain [17]. While these strategies have led to improvements in strength, toughness, or extensibility individually, their toughness remain subpar (usually less than 100 MJ m^{-3}) compared to anisotropic counterparts. Therefore, achieving a high level of simultaneous toughness, stretchability, and isotropic mechanical performance in a single, scalable aqueous processing route remains a major challenge.

To overcome this challenge, salting-out emerges as a promising strategy due to its ability to promote network densification and intermolecular bonding without introducing directional bias [18]. The salting-out process exploits Hofmeister effects, where specific ions disrupt polymer-solvent interactions and drive phase separation, facilitating hydrogen bonding and crystallite formation among polymer chains [19]. Specifically, anions with high charge density strongly bind water molecules, forming thick and tightly held hydration shells, which expels water away from the polymer's hydration layer, weakening polymer–water interactions and promoting polymer-polymer interactions. These crystallites serve as strong physical crosslinks that enhance energy dissipation across the polymer matrix and significantly improve the mechanical properties. However, premature formation of hydrogen bonds and chain aggregation can occur during the early stages of the gelation process, which hinders development of a uniform network and arrests the polymer chains in suboptimal configurations. This leads to inhomogeneous network architectures with localized stress concentrations, which ultimately compromise the mechanical properties of the hydrogel [20].

To further improve the toughness of hydrogels without introducing mechanical anisotropy, alternative methods like solvent exchange [21, 22] or synthesis of near-ideal networks [23, 24] have been employed, focusing on homogenization of the polymer network to prevent stress concentration. For example, polymers like polyvinyl alcohol (PVA) are first dissolved in a good solvent such as dimethyl sulfoxide (DMSO) to enhance polymer–solvent interactions, preventing premature bonding between chains and favoring homogeneous chain distribution, followed by immersion in water to trigger phase separation and interpolymer hydrogen bonding [25]. Similarly, ionic repulsion between protonated functional groups can prevent non-covalent bonding between polymer chains and facilitate uniform dispersion of polymers [26]. For instance, highly soluble short-chain chitosan is integrated into a polyacrylamide hydrogel, which is subsequently immersed in an alkaline solution to deprotonate the amide groups in chitosan and eliminate ionic repulsions, inducing physical crosslinking via hydrogen bonding, hydrophobic interactions and crystallite formation [27]. In addition, such a strategy could be applied to PVA by deprotonating its hydroxyl groups with a strong base to prevent hydrogen bonding and promote more extended conformation, followed by reprotonation to drive nucleation of fine crystallites [28]. In addition, near-ideal homogeneous network has been synthesized from Tetra-PEG macromonomers to minimize structural defects and improve mechanical properties [23]. Although these techniques have successfully improved network uniformity, the achievable mechanical enhancement still remains modest, possibly due to the insufficiently strong intermolecular interactions. Consequently, it poses a significant challenge to establish a uniform network structure that is fixed by strong crosslinking in order to achieve hydrogels with ultra-high toughness.

In this work, we propose a novel strategy to fabricate tough and mechanically isotropic hydrogels by synergistically modulating polymer chain mobility and physical crosslinking throughout the gelation process. This is achieved by manipulating the interchain interactions via sequential steps of acidification, freeze-thawing, and salting-out. Specifically, we acidify the PVA precursor solution to protonate hydroxyl groups [29], thereby weakening intermolecular hydrogen bonding, enhancing chain mobility, and preventing premature aggregation in the solution. This acid-mediated weakening of physical interactions causes a homogenized chain distribution and facilitates the formation of a uniform network architecture (Figure 1). A following freeze-thawing step introduces minimal physical crosslinking to form a gel and preserve its structural integrity in preparation for the subsequent salting-out step. Upon immersion in specific salt solutions, the previously protonated hydroxyl groups would be deprotonated by the basic solution, restoring their ability to form strong hydrogen bonds. Simultaneously, the salting-out process occurs, leading to controlled crystallization, during which the mobile chains densely pack into hydrogen-bonded crystalline domains. These crystallites act as strong physical crosslinks, effectively dissipating mechanical energy and improving network cohesion.

The resulting hydrogels exhibit exceptional mechanical performance, achieving tensile strength of 29.5 MPa, stretchability of 2684%, fatigue resistance of 4.46 kJ m^{-2}, and toughness of 424 MJ m^{-3}, well exceeding the benchmarks of isotropic and even many anisotropic tough hydrogels in their reinforced direction. More importantly, the mechanical properties are isotropic, making the material suitable for demanding applications involving multidirectional mechanical stress. We further demonstrate that

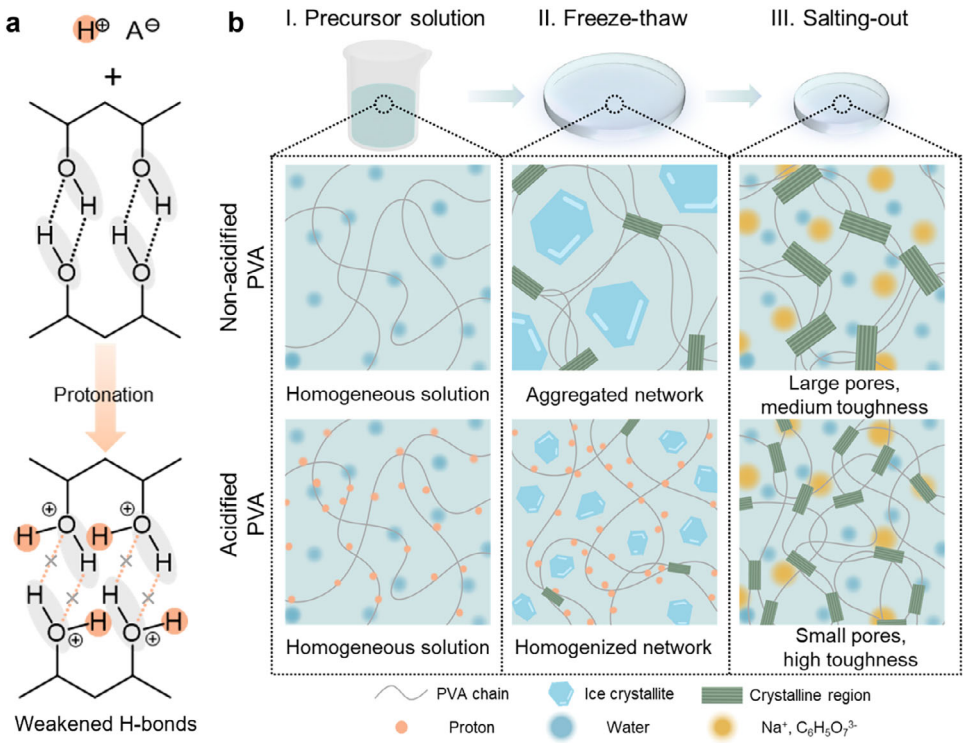

FIGURE 1 | Schematic diagram of fabricating strong and tough PVA hydrogel via acidification, freeze-thaw cycles, and salting-out. (a) Hydroxyl groups in PVA can be protonated to destabilize the intermolecular hydrogen bonds between PVA chains, improving the chain mobility. (b) Synthesis of PVA hydrogel with non-acidified and acidified precursor solution. PVA macromolecules are solvated in water to form a homogeneous solution, gelated during freeze-thaw cycles, and toughened after salting-out in a sodium citrate solution.

this method is generalizable to other polymer systems beyond PVA, and is compatible with additive manufacturing techniques, highlighting its potential as a versatile and scalable strategy for future hydrogel-based devices. By integrating control over both network uniformity and intermolecular interactions, this approach paves a new way in the rational design of tough, functional hydrogels.

2 | Results and Discussion

Mechanically tough and strong hydrogels were synthesized via a three-step process of precursor acidification (step I), freeze-thawing (step II), and salting-out (step III). Briefly, in step I, a stock solution of PVA was prepared by dissolving PVA powder in 90°C water, which was subsequently diluted using water and 37% HCl to produce a homogeneous precursor solution with desired concentration of PVA and acid (Figure 1b). The precursor solution underwent freeze-thaw cycles (−20°C and room temperature) in step II to form a soft and weak gel (termed as PVA-FT gel) with slight physical crosslinking, during which the nucleation of ice crystals during freezing promoted aggregation of polymer chains, inducing formation of intermolecular hydrogen bonding between hydroxyl groups in PVA macromolecules. Acidification of the precursor weakens and decreases the number of hydrogen bonds, increasing the chain mobility to facilitate chain rearrangement to more uniform network structures. The protonation of PVA molecules was confirmed using potentiometric titration, where acidified PVA was titrated against a base solution. Two inflection points were observed, corresponding to the neutralization of excess acid and protonated PVA, respectively (Figure S1) [29]. During step III, the freeze-thawed gel is immersed in sodium citrate solution to deprotonate the oxonium cations to restore its ability to form hydrogen bonds, while yielding a salting-out effect that causes strong physical crosslinking between polymer chains, which fixes the highly uniform network structure. These interactions lead to further aggregation of PVA, obtaining a strong and tough hydrogel (termed as PVA-SO gel).

We investigated the influence of composition on the mechanical properties of hydrogels fabricated using the acidification and salting-out by varying the acid concentration, acid species, and PVA concentration (Figure 2a–c). Samples with different acid concentrations and species are denoted as mAcid-PVA, where m is the molar amount of the acid per kilogram of the precursor solution. For example, 1HCl-PVA represents a sample in which 1 kg of precursor solution contains 1 mole of HCl. Representative stress-strain curves of hydrogels with a fixed PVA concentration of 10 wt% acidified with HCl are plotted in Figure 2a, with HCl concentration chosen as 0, 0.1, 0.5, 1, 1.5 and 2 mol kg^{-1} (calculated vs. weight of solution, unless specified otherwise), and ultimate tensile strength, stretchability, and toughness are summarized in Figure 2e–g. As the HCl concentration increases from 0 to 1 mol kg^{-1}, the ultimate tensile strength increases by 73% from 15.4 ± 1.7 to 26.7 ± 2.1 MPa, while the toughness shows a similar trend (143 ± 37 MJ m^{-3} at 0 mol kg^{-1} to 224 MJ m^{-3} at 1 mol kg^{-1}, representing a 57% increase), indicating the effective strengthening and toughening of hydrogel via acidification. Meanwhile, the stretchability improves slightly from 1555% to 1650%. We hypothesize that this trend could be explained as

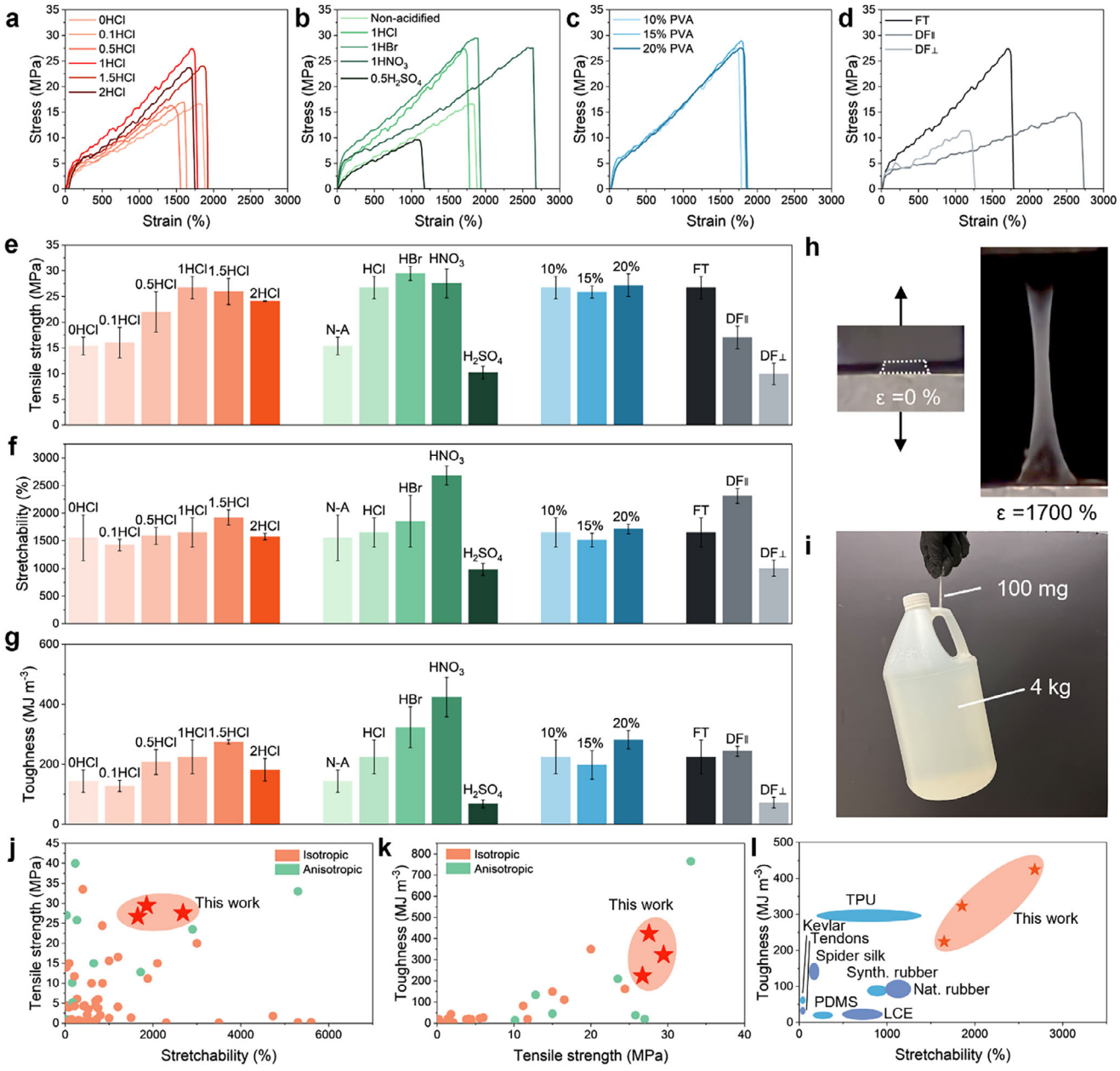

FIGURE 2 | Mechanical properties of PVA hydrogels. Representative stress-strain curves of PVA hydrogels fabricated using precursor solutions with (a) HCl concentration from 0 to 2 mol per kilogram of solution, (b) different acid species while nominal concentration of protons kept constant, and (c) PVA concentration from 10 to 20 wt.%. (d) Representative stress-strain curves of PVA hydrogels synthesized using freeze-thaw cycles and directional freezing (stretched in the parallel or perpendicular direction to the nanofibrils). (e-g) Summary of (e) tensile strength, (f) stretchability, and (g) toughness of different PVA hydrogels. (h) Photographs of 1HCl-PVA-SO gel before and after stretching. The gel did not break when stretched to 1700% strain. (i) Photograph of 1HCl-PVA-SO gel (100 mg) lifting a weight of 4 kg (~40 000 times of body weight) without breaking. (j,k) Ashby diagrams of (j) tensile strength vs. stretchability, (k) toughness vs. tensile strength, and (l) toughness vs. stretchability of hydrogel reported in this work and other reported tough hydrogels and polymers [7, 8, 11–13, 15, 19, 25, 27, 31–77].

follows. If no HCl is added, the large ice crystals formed during freezing squeezed the PVA chains into condensed pore walls, and hydrogen bonding between hydroxyl groups on PVA chains will cause significant physical crosslinking in the PVA-FT gel, resulting in local chain aggregation and crystallites. This leads to highly nonuniform microstructure featuring large pores and dense pore walls. By contrast, in acidified PVA solution, hydroxyl groups will be protonated and form delocalized oxonium cations ($-OH_2^+$), shielding the partial negative charge on the oxygen atom. Consequently, the protonation of PVA chains leads to weaker and less hydrogen bonding and higher chain mobility (Figure 1a). As a result, the PVA chains in the freeze-thawed gel become highly flexible and evenly distributed without being pinned by crystallites, enabling the formation of uniform network structures. Meanwhile, the amount of physical crosslinking is large enough to ensure that the PVA-FT gel remains in the gelated state when immersed in a salt solution instead of dissolving. A higher concentration of HCl leads to a larger fraction of hydroxyl

groups in PVA chains being protonated, causing less crystalline regions to form that pins the motion of PVA molecules in the PVA-FT gel (Figure S2). Consequently, the polymer chains could freely migrate, allowing for more crystallites to form in the salting-out step. The ultimate tensile strength reaches a plateau at higher acid concentrations of 1.5 and 2 mol kg^{-1}, which can be attributed to the fact that most hydroxyl groups have already been protonated at an HCl concentration of 1 mol kg^{-1}. The concentration of 1 mol kg^{-1} was chosen for further characterizations, because at higher acid concentrations the FT gel would become very soft and difficult to handle due to excessive suppression of physical crosslinks, even though the toughness of SO gel reaches maximum value at 1.5 mol kg^{-1}. This behavior will be discussed further in the subsequent sections.

Additionally, the anion species of acid plays a critical role in affecting the interaction between polymer, water, and ions in the solution, suggesting a complex coupling between protonation and Hofmeister effect in both freeze-thawing and salting-out process (Figure 2b,e). The HCl in PVA (10 wt%) precursor was replaced with nitric acid (HNO_3), hydrobromic acid (HBr), or sulfuric acid (H_2SO_4) while keeping the nominal concentration of protons constant at 1 mol kg^{-1}. It has been previously reported that the salting-out effect of anions has an order as follows: $SO_4^{2-} > Cl^- > Br^- \approx NO_3^-$[18]. In agreement with this series, we observed that the compression modulus of PVA-FT gels with different acid species has the order of $0.5H_2SO_4 >> HCl > HBr > HNO_3$ (Figure S3). Despite the similar nominal salting-out strength of Br^- and NO_3^-, we find that NO_3^- leads to the greatest stretchability and toughness of the SO gels. We assume that the weaker hydration enthalpy of NO_3^- ($\Delta H_{hyd} = -314$ kJ/mol) compared with Br^- (−348 kJ/mol) facilitates its partial insertion near hydroxyl groups, modulating hydrogen bonding more modestly [30]. It may enhance chain mobility and network rearrangement without driving excessive dehydration or premature aggregation. By contrast, Br^- is more strongly hydrated and more prone to form a dense, tightly associated network, which increases strength but reduces extensibility (Figure 2e–g). According to the previous hypothesis, the protonation should hinder the intermolecular hydrogen bonding between PVA chains. However, strong salting-out ions like SO_4^{2-} with a high charge density and small ionic radius, would strongly promote the interaction between PVA molecules and induce aggregation, which contradicts the effect of protonation. Moreover, such premature aggregation is enhanced by the suppression of hydrogen bonding between PVA and water in the acidic environment, which drives further dehydration from the polymer chain. As a result, premature formation of crystallites in PVA-FT gels with these strong salting-out ions like SO_4^{2-} would undermine the mobility of the chains, preventing a uniform network structure. After salting-out in sodium citrate solution, the $0.5H_2SO_4$ gel exhibits much lower mechanical properties than 1HCl gel or even non-acidified samples, possibly due to its highly non-uniform network structure. On the other hand, strong acids with salting-in anions exhibit higher mechanical properties than non-acidified samples, with an order that agrees well with the Hofmeister series, supporting the effectiveness of enhancing chain mobility for toughening the hydrogel. Notably, the $1HNO_3$-PVA-SO sample achieves a record-high toughness of 424 MJ m^{-3} among isotropic hydrogels. In addition, the effect of PVA concentration was also studied. Precursor solutions with PVA concentrations of 5, 10, 15, and 20 wt% were prepared while HCl concentration was fixed at 1 mol kg^{-1}. PVA solution with a low concentration of 5 wt% did not gelate after 4 freeze-thaw cycles and dissolved into a cloudy solution when soaked into the sodium citrate solution. When the PVA concentration increases from 10 to 20 wt.%, the tensile strength, stretchability and toughness of the hydrogel exhibit a non-monotonic trend (Figure 2c), which slightly decreased at 15 wt.% before rising again at 20 wt.%. This behavior can be attributed to two effects. First, during the salting-out step, the polymer chains condense into a homogeneous polymer-dense phase, whose final polymer concentration and network structure become similar regardless of the starting composition. Second, at higher initial concentrations (15–20 wt.%), solution viscosity rises sharply, which impedes homogeneous ion/acid diffusion, chain rearrangement and uniform network formation, leading to defects and reduced performance at 15 wt.%. At 20 wt.%, the increased chain entanglements recover some mechanical performance, but the workability is significantly compromised by its high viscosity. For practical processing and balanced mechanical performance, we selected 10 wt.% PVA for further characterization unless otherwise specified.

We further explored the effect of freezing conditions on the mechanical properties of the hydrogel. When no freezing was conducted, directly adding the salt solution into the precursor only yielded a turbid slurry, proving the necessity to include a freeze-thaw process to form a lightly crosslinked gel to preserve its macroscopic structure before salting-out. The freezing temperature was changed from −5°C to −80°C (Figure S4). Gels that underwent freeze-thaw cycles at −5°C collapsed, attributed to insufficient physical crosslinking. When freezing temperature decreased from −20°C to −80°C, the tensile strength remained stable, but the stretchability and toughness dropped significantly (1650%, 224 MJ m^{-3} at −20°C to 920%, 177 MJ m^{-3} at −80°C). This trend can be ascribed to the higher crystallinity of PVA-FT gels frozen at lower temperatures, as the crystallites serve as crosslinking points that prevent the motion of polymer chains, counteracting the effect of acidification. Additionally, a control hydrogel was prepared via directional freezing (DF) followed by salting-out. During directional freezing, ice nucleation occurs preferentially along an externally exerted temperature gradient in a cooling bath to yield polymer nanofibrils that are aligned with the temperature gradient. The DF hydrogel exhibits significantly contrasting mechanical properties when stretched in the direction parallel or perpendicular to the aligned nanofibrils—the tensile strength, stretchability, and toughness of the DF gel (10 wt.% PVA-1HCl) stretched in the parallel direction (17.0 MPa, 2312%, 243 MJ m^{-3}, respectively) are higher than in the transverse direction (10.0 MPa, 1002%, 72 MJ m^{-3}, respectively), while no orientation-dependence of mechanical properties is observed in the hydrogels prepared via freeze-thawing. It is also noteworthy that the acidified PVA precursor yields PVA-SO gels of greater mechanical properties than our previously reported unacidified hydrogel made via either freeze-thawing or directional freezing (in the parallel direction). We demonstrate the superior mechanical properties by showing that the 1HCl-PVA-SO gel can be stretched to 1700% without fracturing (Figure 2h) and withstand a load that is approximately 40 000 times of its own weight (Figure 2i). Furthermore, this hydrogel shows tensile strength comparable to state-of-the-art tough and strong hydrogels synthesized with double network, dual crosslink, solvent-exchange,

and so forth. The stretchability of our hydrogel is also higher than most of these reported examples. Most importantly, our hydrogel reaches record-high toughness among all hydrogels reported to this date and easily surpasses that of synthetic rubbers and tendons (Figure 2j–l).

To investigate the effect of protonation on the PVA in an acidic environment and to support the hypothesis that protonation may inhibit intermolecular hydrogen bonding between PVA chains, we conducted reactive molecular dynamics (MD) simulations using the ReaxFF C/H/O/Li/Na/K/Cl/I force field re-parameterized based on previous reports [78, 79]. Specifically, to explore the protonation mechanism of the PVA dimer, we placed a PVA dimer with 20 -OH groups in both neutral (H_2O) and acidic (HCl solution) environments (Figure S5) and performed an initial NVT (constant temperature and volume) equilibration at 300 K for 2.0 ns. To study the morphological changes and the evolution of the hydrogen bond network in the PVA dimer during the freeze-thawing process, we carried out a second NVT equilibration at 253 K for an additional 2.0 ns. Details of the modeling and MD simulation are provided in Text S1.

In the first equilibration at 300 K, we observed decomposition of HCl and proton transfer between H_2O molecules, leading to the formation of Cl^- and H_3O^+ (Figure S6), followed by subsequent proton transfer from H_3O^+ to PVA-OH groups to form -OH_2^+ and H_2O (Figure S7). The protonation of PVA-OH groups was also supported by a shift of the proton on methine group, which hydroxyl group attached to, toward the high-field direction with higher acid concentrations in the NMR (nuclear magnetic resonance) spectra (Figure S8). During the second equilibration at 253 K, the two chains of the PVA dimer remained aligned in the neutral environment (H_2O), whereas one chain tended to coil in the acidic environment (HCl solution) (Figure 3a,b), with an approximately 5.0 Å shorter head-to-tail distance (Figure 3c; Figure S9). The degree of alignment between the two chains can be further evaluated by analyzing the nearest C—C and O—O distances (Figures S10 and S11). As shown in Figure S10a, the C—C nearest distances in the PVA dimer equilibrated in H_2O were more evenly distributed along the carbon backbone (< 6.0 Å). In contrast, the C—C nearest distances in the HCl solution are significantly larger at the two chain ends, exceeding 6.0 Å or even reaching 8.0 Å, consistent with the higher degree of curling of the PVA dimer. In comparison, the nearest O—O distances (Figure S10b) show no significant difference between the neutral and acidic cases, as the —OH groups have higher mobility relative to the carbon backbone. Reference lines at 3.4 Å were included to identify O—O pairs that could potentially form intermolecular hydrogen bonds between the two chains. The number of O—O pairs falling below this cutoff was approximately the same in both the neutral and acidic systems, suggesting that the geometric availability for intermolecular hydrogen bonding was similar, regardless of the potential weakening of bond strength due to protonation of —OH groups (Figure 3d). Quantification of intermolecular hydrogen bonds between the two chains of PVA dimer shows similar counts in H_2O and HCl solutions when accounting for bonds contributed by —OH_2^+ groups (Figure 3e). At 2.0 ns, ~37.5% of —OH groups in the HCl solution were protonated (Figure S12b), with ~50% of hydrogen bonds involving –OH_2^+ at the end of equilibration (Figure 3e; Figure S12c). Based on these simulation results, we infer that the curling of the PVA dimer in acidic environment was caused by the weakening of intermolecular hydrogen bonds involving —OH_2^+ groups, resulting in higher chain mobility and a more uniform distribution, as observed experimentally.

While ReaxFF using the Electronegativity Equalization Method (EEM) [80] can provide reasonable qualitative insights and track trends in charge transfer, polarization, and changes in the local environment during reactions, high-level quantum mechanical (QM) calculations are needed to obtain quantitative and more accurate atomic charges for hydrogen bond analysis. To validate our hypothesis that protonation weakens intermolecular hydrogen bonding,, we performed non-periodic DFT calculations using the Schrödinger Jaguar software package [81] to determine the intermolecular hydrogen bond strengths between (1) two —OH groups, (2) one —OH_2^+ and one —OH (with —OH_2^+ initially as acceptor), (3) one —OH_2^+ and one —OH (with —OH as acceptor), and (4) two —OH_2^+ groups (Figure S14a,c,e,g).

To exclude interactions from nearby atoms of the PVA chains and solvent molecules, we employed dry C_3H_7OH dimers with different protonation states as the initial geometries for ReaxFF and DFT minimizations. A comparison of the intermolecular hydrogen bond strengths obtained from ReaxFF and DFT calculations is presented in Figure 3f. For Case 1, the hydrogen bond strength between the two neutral —OH groups showed good agreement between ReaxFF and DFT. For partially protonated dimers (Cases 2 and 3), both methods indicated a comparable or stronger hydrogen bond than in the neutral case, due to emergence of a symmetric proton-sharing geometry according to DFT minimizations (Figure S15a). In Case 4, the ReaxFF result suggested an extremely weak interaction, with a minimized distance greater than 40.0 Å (Figure S14), whereas the DFT calculation yielded a positive interaction energy due to strong repulsion.

It should be noted that these calculations using dry dimers capture the intrinsic intermolecular hydrogen bond strength between a pair of —OH/—OH_2^+ groups, but fail to account for proton transfer events, hydration, solvation dynamics, and associated chemical processes in an aqueous environment. These effects were assessed using Mulliken charge of the shared proton as a function of the number of surrounding H_2O molecules, ranging from 1 to 9. As the number of H_2O molecules increased, a solvation shell began to form, stabilizing the oxygen lone pairs. Simultaneously, the proton became increasingly delocalized, as indicated by a decreasing Mulliken charge (Figure 3g), leading to the weakening and eventual disruption of the hydrogen bond. When 8 or more H_2O molecules were present, we observed complete proton transfer, resulting in the formation of a Zundel-type hydrated proton (Figure S15b). In conclusion, hydrogen bonding between —OH and —OH_2^+ groups are unstable in an aqueous environment. Overall, these results reveal the disruption of hydrogen bonding networks caused by solvation of protonated hydroxyl groups, which facilitates higher PVA chain mobility in acidic solution compared to neutral conditions, ultimately contributing to the softening of FT gels and ultimately enhancement of SO gels, as will be discussed in following sections.

We further developed an association model to support the hypothesis of weakened interactions in acidified PVA precursors

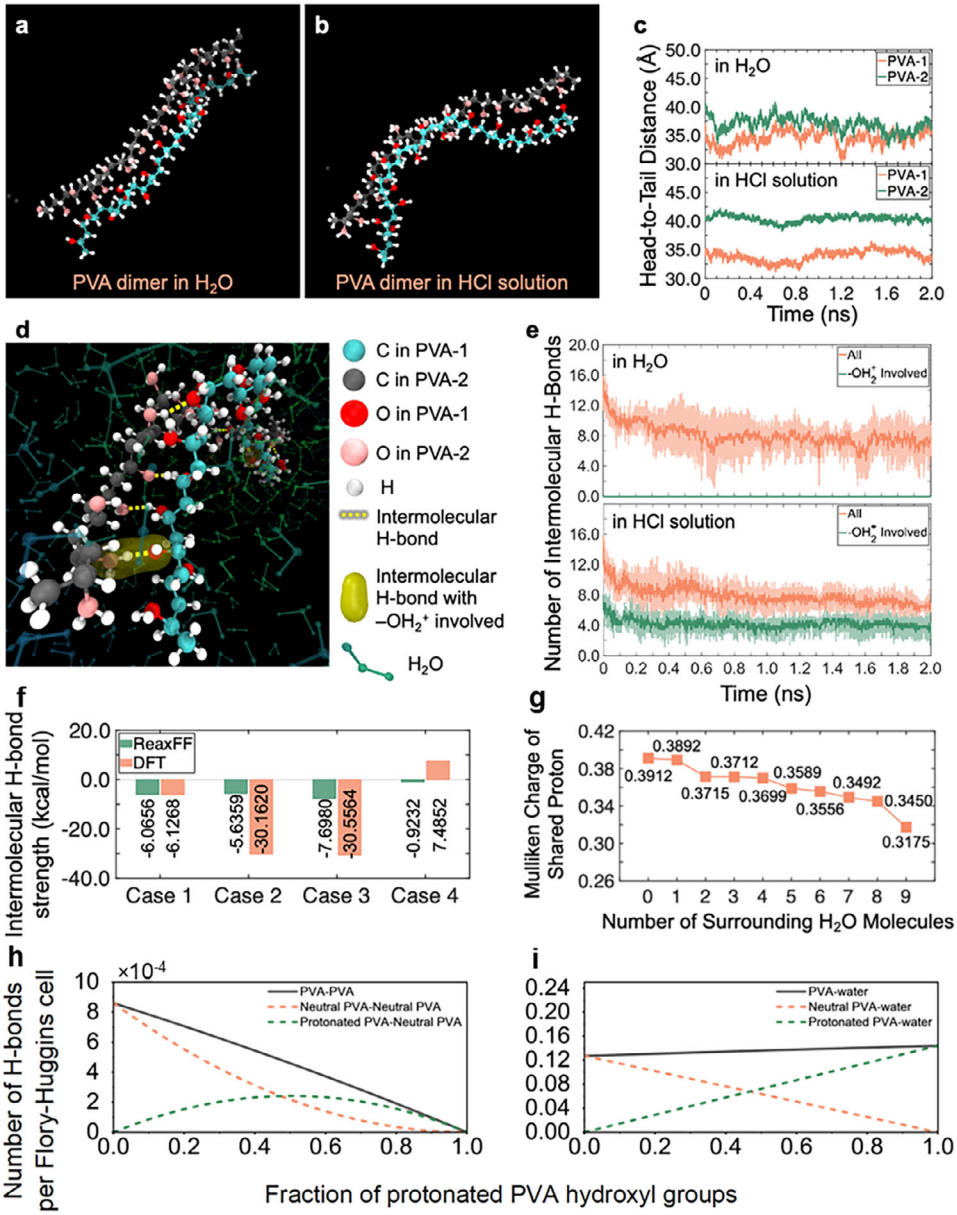

FIGURE 3 | Structural characteristics and hydrogen bonding of PVA dimers in neutral and acidic environments from ReaxFF and DFT calculations. (a,b) Molecular structures of PVA dimers in (a) H_2O and (b) HCl solution extracted from ReaxFF NVT simulations at 253 K and 2.0 ns. (c) Head-to-tail distances of PVA dimers in H_2O and HCl solution during the simulations at 253 K over 2.0 ns. (d) Schematic illustration of intermolecular hydrogen bonds, including those contributed by protonated hydroxyl groups, for the PVA dimer in HCl solution from the simulation at 253 K and 2.0 ns. (e) Time evolution of intermolecular hydrogen bonds, including those contributed by protonated hydroxyl groups, for PVA dimers in H_2O and HCl solution during the simulations at 253 K over 2.0 ns. The solid curves represent averages over three samples run with the same simulation setup for 2.0 ns, and the transparent background curves indicate the standard deviations of those three samples. (f) Comparison of hydrogen bond strengths for Cases 1–4 using ReaxFF and DFT. (g) Mulliken charge variation of the shared proton in the C_3H_7OH dimer configuration as the number of surrounding H_2O molecules increases from 0 to 9. (h,i) Number of hydrogen bonds per Flory-Huggins cell between (h) PVA-PVA molecules and (i) PVA-water molecules according to association modeling.

addressing the number of hydrogen bonds between different species. In the model, the mixture is represented on a Flory–Huggins lattice (Text S2), where each species carries donor and acceptor sites that define the possible hydrogen bonds. Acidification is captured by treating PVA as a binary mixture of neutral hydroxyl and protonated sites, with the latter reducing the available bonding capacity. As acid concentration increases, the number of PVA–PVA hydrogen bonds diminish, weakening interpolymer associations (Figure 3h). Meanwhile, the number of PVA-water hydrogen bonds would increase, which enhances the dispersion of PVA molecules in the solution (Figure 3i).

To experimentally elucidate the strengthening and toughening mechanism, we carefully examined each fabrication step at the multiple length scales. First, the influence of acidification during dissolution on polymer chain conformation is investigated.

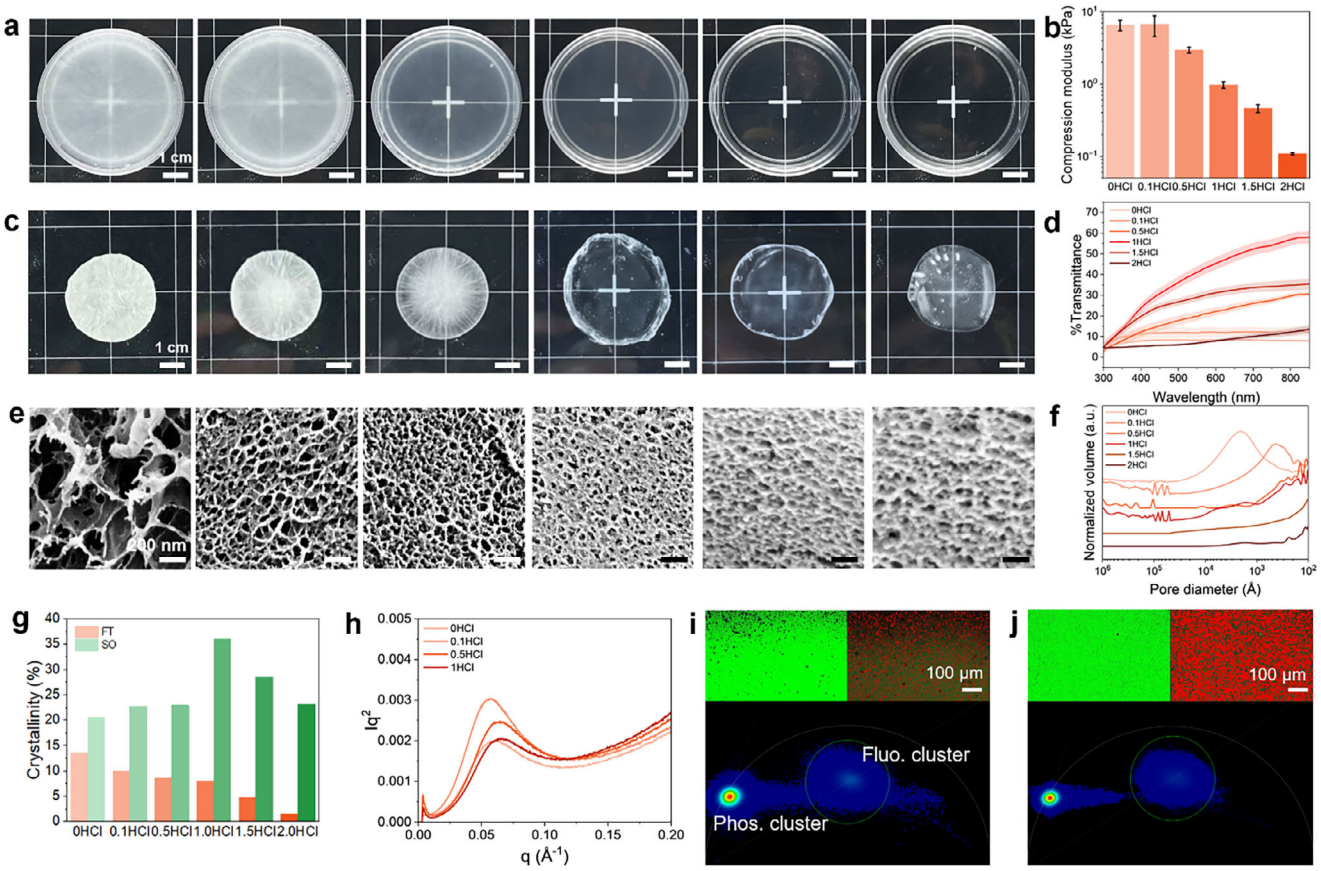

FIGURE 4 | Investigation of the toughening mechanism and microstructure. (a) Optical images of PVA-FT gels. Left to right: 0HCl, 0.1HCl, 0.5HCl, 1HCl, 1.5HCl, 2HCl. Scale bar: 1 cm. (b) Compressive modulus of PVA-FT gels. (c) Optical images of PVA-SO gels. Left to right: 0, 0.1, 0.5, 1, 1.5, 2HCl. Scale bar: 1 cm. (d) Transmittance of PVA-SO gels. (e) SEM images of PVA-SO gels. Left to right: 0, 0.1, 0.5, 1, 1.5, 2HCl. Scale bar: 200 nm. (f) Volume distribution of pore size of PVA-SO gels measured by mercury intrusion porosimetry. (g) Crystallinity of PVA-FT and PVA-SO gels with different acid concentrations measured using DSC. (h) Representative SAXS diagrams of SO gels. (i,j) FLIM images (upper left: fluorescence channel; upper right: phosphorescence channel) and phasor diagrams (bottom) of (i) 0HCl-PVA-SO and (j) 1HCl-PVA-SO gels.

Optical images of 0, 0.1, 0.5, 1, 1.5 and 2HCl-PVA-FT gels and respective compression moduli are summarized (Figure 4a,b). When no acid is present, the hydrogel exhibits a translucent pattern (Figure 4a) resulting from the crystalline domains yielded during the freeze-thaw process, where ice crystals cause the chains to aggregate and crystallize. A higher concentration of HCl in the precursor solution results in more transparent and softer PVA-FT gels, supporting that crystallite formation during freeze-thaw cycles is hindered by the addition of HCl, attributed to the suppression of hydrogen bonding when hydroxyl groups are protonated, as suggested by the MD simulations. In short summary, the acidification step homogenized the network distribution in the aqueous solution, and the freeze-thaw step introduced a minimal amount of physical crosslinks to fix such chain conformation and maintain the shape of the hydrogel to prepare it for the final salting-out step. As PVA macromolecules are allowed to move more freely due to less crystallites in acidified PVA-FT gels, it is expected that the chains will be more evenly distributed, which has a profound effect on the pore structure of PVA-SO gels in step III. Specifically, a similar trend of transparency for PVA-FT gels is observed, as 0HCl-PVA-SO appears opaque while 2HCl-PVA-SO gel is translucent (Figure 4c). UV–vis spectroscopy measurements confirm the much lower transmittance of 0HCl-PVA-SO gel (~8% at 500 nm) than 1HCl-PVA-SO gel (Figure 4d), suggesting less scattering of visible light in the hydrogel, which further indicates that the pore size might be smaller than the wavelength of visible light. The transmittance decreases for samples with higher acid concentrations, which is possibly attributed to the wrinkles generated in the excessively soft FT gels during salting out. Scanning electron microscopy (SEM) images (Figure 4e) of 0HCl-PVA-SO gel shows that it has an average pore diameter of approximately 500 nm. By contrast, 1, 1.5, and 2HCl-PVA-SO gel has a much smaller pore size of 10–20 nm and a uniform network structure. The trend of pore size is supported by mercury intrusion porosimetry (MIP) measurements, where the pore diameter at peak normalized volume decreases as the acid concentration increases (Figure 4f). The trend in pore size is consistent with our previous hypothesis: acidified PVA chains have higher flexibility such that they diffuse and rearrange more freely in the PVA-FT gel. Consequently, their network structures are more evenly distributed, which are fixed during salting-out, leading to smaller pores. Interestingly, despite the distinct pore size distributions of gels with different acid concentrations, MIP reveals that the porosity (volume fraction of voids in a bulk gel) of these gels is extremely close to each other (~88%) (Figure S16). This observation is in agreement with the fact that the polymer dense phase precipitated from a phase separation should have a stable composition regardless of the

composition of the parent phase. In conclusion, the salting-out step further densifies and fixes the chain conformation to yield an isotropically tough hydrogel.

Second, we verified if the high chain mobility brought by acidification can contribute to the strong physical crosslinking during the salting-out process. Differential scanning calorimetry (DSC) detects endothermic peaks in the range of 200°C – 250°C, which is assigned to the melting of PVA crystals. When HCl concentration increases up to 1 mol kg^{-1}, the crystallinity of PVA-FT gels calculated from DSC curves becomes lower, verifying that HCl impedes crystallite formation. At higher HCl concentrations, the crystallinity decreased, which might be attributed to incomplete deprotonation during salting out. Since the high flexibility of acidified PVA molecules should allow for better packing of chains in the salting-out process, a decreasing trend of crystallinity of PVA-FT gels is observed—all PVA-SO gels have improved crystallinity compared to their PVA-FT gel counterparts, while a higher HCl concentration translates to higher crystallinity in PVA-SO gels (Figure 4g; Figure S17). Such trend was supported by water content tests (Figure S18), which shows that FT gels with higher initial acid concentrations, after washing away the acid, have higher water content due to less physical crosslinks. Meanwhile, the trend is reversed for SO gels, with a higher initial acid concentration leading to lower water content that reached a plateau at 1 mol kg^{-1}, suggesting higher crosslink density, which is consistent with our hypothesis that acid facilitates crystallite formation during salting out. SAXS results indicate a right shift in the peak scattering vector with higher HCl concentration, suggesting a smaller average distance between crystals, and thus a higher density of physical crosslinks (Figure 4h; Figure S19). The crystalline regions are visualized using fluorescence lifetime imaging microscopy (FLIM) with phasor approach. A chromophore Bis-BrNpA was doped into the hydrogel; it exhibits only fluorescence in solution, but emits both fluorescence and phosphorescence when confined within crystalline regions. The 0HCl-PVA-SO and 1HCl-PVA-SO samples exhibit similar brightness in the fluorescence channel (400–470 nm), revealing similar fluorescence lifetime of 1.21 and 1.25 ns, respectively (Figure 4i,j, upper left). Meanwhile, the acidified sample shows greater brightness in the phosphorescence channel (510–580 nm), with a longer lifetime of 6.48 ns compared to 5.99 ns of non-acidified sample, indicating a larger density of crystals and a strong intermolecular interaction in the crystalline region (Figure 4i,j, upper right). Additionally, the phasor diagram of the acidified gel shows a smaller phosphorescence cluster, suggesting a more uniform distribution of distance between crystalline regions (Figure 4i,j, bottom), conducive to the stress distribution among polymer chains. Furthermore, to rule out the effect of any potentially formed chemical crosslinking under heat or strongly acidic environments [82–84], we compared the NMR spectra of a low-molecular weight PVA (M_w = 9000) dissolved at room temperature and a high-molecular-weight PVA (M_w = 89000) dissolve at 90°C (Figure S20). In case of chemical crosslinking, the signal for methine hydrogen should be shifted, while for both samples it appeared at a chemical shift of 3.94 ppm, indicating minimal chemical crosslinking occurred even when PVA was dissolved at an elevated temperature. Additionally, we immersed PVA-SO gel in DMSO at room temperature after washing away the salt with water, which completely dissolved after 6 h (Figure S21), indicating minimal chemical crosslinks have formed during the whole fabrication process that could potentially contribute to the mechanical performance.

To further confirm the toughening mechanism via improving chain flexibility, control samples were prepared by replacing HCl with salts with strong salting-in effects including magnesium chloride ($MgCl_2$), copper chloride ($CuCl_2$), and iron chloride ($FeCl_3$). Salting-in ions improve the solubility of polymer macromolecules in water by disrupting the hydrogen bonding between water molecules. Therefore, it is anticipated that these salts should have a similar effect of improving the chain flexibility of PVA molecules in PVA-FT gel. Due to the strong salting-in effect, 1$MgCl_2$-PVA precursor failed to gelate after 4 freeze-thaw cycles. For other precursors with salt added except 1$FeCl_3$, the PVA-SO gels were toughened to different extents compared to the gel without acid or salts (Figure S22), which supports the proposed strategy of network homogenization before salting-out. However, for the 1$FeCl_3$-PVA-SO sample, the high concentration of Fe^{3+} ions formed dark brown $Fe(OH)_3$ precipitates in the hydrogel matrix when it came in contact with the basic sodium citrate solution. Therefore, the hydrogel is severely embrittled by the precipitate particles, leading to poor mechanical properties.

We further studied the reversibility of the acidified hydrogel under cyclic loading. A relatively large hysteresis was observed, indicating large energy dissipation during deformation, which is assigned to the breaking of a large amount of sacrificial bonds (hydrogen bonds) (Figure 5a,b). We also confirmed that these hydrogen bonds are partially recoverable by stretching the hydrogel for multiple cycles with progressively larger strains (Figure S23a). We observed that the loading curve of each new cycle does not follow the unloading curve of the previous cycle, indicating that some of the physical crosslinks have reformed and contribute to strength recovery. By estimating the recoverable fraction as the overlapping area between two consecutive loading-unloading loops divided by the area of the prior loop, we found that approximately 30% of these interactions recover over the timescale of the test (Figure S23b). To further utilize the reversibility of the physical crosslinks, we conducted cyclic tensile tests with 5 min of resting at stress-free state between each cycle (Figure S24). The sample exhibited consistent stress-strain curves after the first conditioning cycle and minimal residual strain after each resting process, demonstrating good reversibility and consistently large toughness, making it particularly useful for applications with non-continuous large loading. The fatigue resistance of the material is also crucial for real-life applications where it is often subjected to dynamic loads. Notably, the 1HCl-PVA-SO gel reaches a high fatigue threshold of 4.46 kJ m^{-2} (Figure 5c). To validate the fatigue threshold, a notched sample was cycled at an energy release rate of 4.10 kJ m^{-2} for 5000 cycles, and no crack propagation was observed (Figure 5d). Furthermore, we demonstrate that our strengthening and toughening strategy can be generalized to other polymers with protonatable functional groups. Gelatin is used as a model polymer, which contains primary amine groups from arginine moieties that can be readily protonated. We are able to improve the tensile strength by 408% (0.42 to 2.13 MPa) and toughness by 768% (0.20 to 1.74 MJ m^{-3}) by increasing HCl concentration from 0 to 1 mol kg^{-1} (Figure 5e,f; Figure S25).

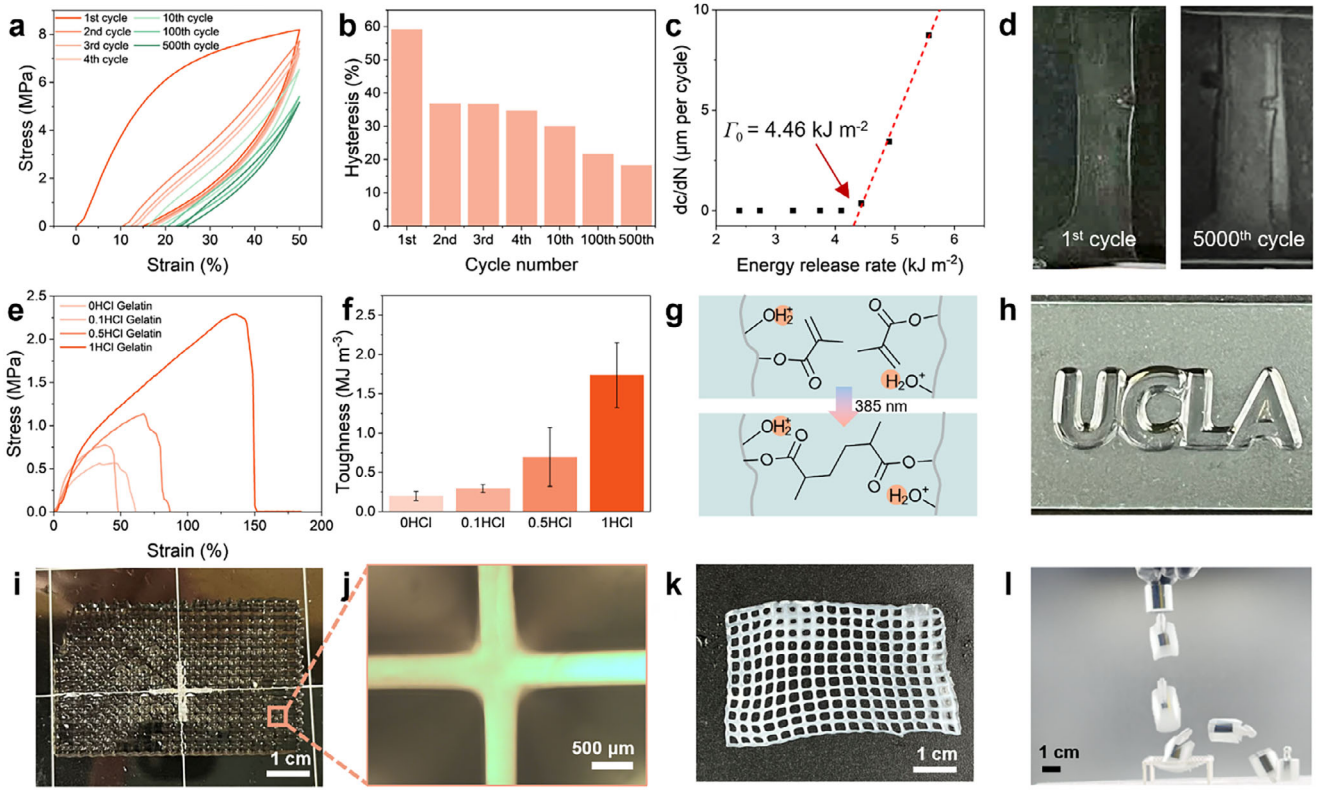

FIGURE 5 | Fatigue resistance and generality of acidified hydrogel. (a) Stress–strain curves of 1HCl-PVA-SO gel under cyclic loading to 50% strain from 1 to 500 cycles. (b) Mechanical hysteresis of the 1HCl-PVA-SO gel from under cyclic loading to 50% strain from 1 to 500 cycles. (c) Fatigue resistance of 1HCl-PVA-SO gel. (d) Validation of the fatigue threshold at 4.10 kJ m^{-2} for 1HCl-PVA-SO gel using the single-notch test. Photos are taken at the first and the 5000th cycle. Scale bare: 2 mm. (e) Representative stress-strain curves of 10 wt.% 0, 0.1, 0.5, and 1HCl-Gelatin-SO hydrogels. (f) Toughness of 10 wt.% 0, 0.1, 0.5, and 1HCl-Gelatin-SO hydrogels. (g) Schematic of poly(vinyl alcohol methacrylate) (PVAMA) photocrosslinked under 385 nm light. (h) Photograph of printed PVAMA hydrogel with UCLA pattern. Scale bar: 1 mm. (i) Photograph of printed PVAMA hydrogel with grid pattern. Scale bar: 1 cm. (j) Optical microscope image of printed PVAMA hydrogel. Scale bar: 500 μm. (k) Photo of the PVAMA hydrogel net after salting-out. (l) Time lapse image of the PVAMA hydrogel net surviving the impact of a 50 g weight dropped from a 10 cm height.

To better utilize the toughened hydrogel as a structural material, it is often necessary to modify the material into a predesignated shape. Herein, by incorporating photo-crosslinkable functional groups like methacrylate into the polymer, we are able to print tough hydrogels using the same acidification strategy with arbitrary shape via digital light processing (DLP) (Figure 5g,h). For example, a pattern of UCLA logo can be printed using a methacrylate derivative of PVA (PVAMA) as shown in Figure 5g. Similarly, a fishnet structure can be printed featuring a line width as narrow as 0.36 mm with clear boundaries (Figure 5i,j). After freeze-thawing and salting-out the printed 1HCl-PVAMA sample (Figure 5k), the hydrogel fishnet (∼1 g) can survive the impact of a 50 g weight dropping from a 10 cm height, successfully showcasing its remarkable tensile strength and toughness (Figure 5l).

3 | Conclusion

In this study, we developed a three-step process of protonation, freeze-thawing, and salting-out to achieve superior mechanical properties (tensile strength, stretchability, and toughness) in isotropic PVA hydrogel. Guided by the MD simulation, it was elucidated that during the fabrication, protonation improves PVA chain flexibility by suppressing hydrogen bonding to create highly homogenized chain conformation during freeze-thaw cycles, which can be fixed by strong physical crosslinking via salting-out. The ultrahigh toughness of our hydrogel primarily derives from its exceptional extensibility, which enables unique opportunities in soft, deformable systems, such as stretchable actuators, adaptive skins, and wearable elastic substrates, where materials often must accommodate large mechanical deformations repeatedly without rupturing and have adequate modulus to make it easy to actuate and conform through deformation. Beyond PVA, such a strategy can be applied to other polymers with protonatable functional groups, including gelatin, opening possibilities for broader applications like medicine, soft robotics, and additive manufacturing. We also recognize that while the salting-out strategy endows PVA hydrogels with exceptional mechanical robustness, their high residual ion content and susceptibility to dehydration remain important challenges for practical application. These factors may limit direct biomedical use and long-term environmental stability. Future work will focus on mitigating these issues through the incorporation of biocompatible salts and design of water-retentive or encapsulated structures [85–91], thereby extending the applicability of this tough yet versatile hydrogel system.

4 | Experimental Section

4.1 | Materials and Instruments

Poly(vinyl alcohol) (PVA) (weight-average molecular weight (M_w) of 89–98 kDa; degree of hydrolysis of 99%), methacrylic acid (99%), hydroquinone, and sodium citrate tribasic dihydrate were purchased from Sigma–Aldrich. Lithium phenyl-2,4,6-trimethylbenzoylphosphinate (TPO-Li) was purchased from CPS Polymers. Glutaraldehyde (50 v%), hydrochloric acid (36.5–38 wt.%), sodium hydroxide, nitric acid (68–70 wt.%), sulfuric acid (95–98 wt.%), phosphoric acid (85 wt.%), lithium chloride, lithium iodide, and phosphate buffer solution, triethylamine, and acetone were purchased from Fisher Scientific.

The universal mechanical tester model used for tensile and cyclic testing is the UniVert from CellScale. The dynamic mechanical analyzer used for compression tests is the DMA 850 from TA Instruments. The differential scanning calorimeter used for crystallinity measurements was the DSC 250 from TA Instruments. The mercury intrusion porosimeter used for pore size and porosity analysis was the PoreMaster 33 from Anton Paar. The scanning electron microscope model used for morphology imaging was the Supra 40VP from ZEISS. The UV–vis spectrophotometer used for absorbance and optical measurements was the UV-3101 PC from Shimadzu. For directional freezing experiments, the cooling bath system referenced was model PSL1810 from EYELA. Non-periodic density functional theory (DFT) calculations were performed using the Schrödinger Jaguar 10.4 software package.

4.2 | Fabrication of Hydrogel

The acidification step is completed during the preparation of the precursor solution. Specifically, 15, 17 and 23 wt.% PVA stock solutions were prepared by dissolving PVA powder in deionized water at 90°C with vigorous stirring. The stock solutions were cooled to room temperature and then diluted to 5, 10, 15, 20 wt.% precursor solutions using water and desired amount of acid or salting-in salt. The precursor solutions were thoroughly mixed, and air bubbles were removed by centrifugation. 10 wt.% gelatin precursor solution was prepared similarly by diluting a 15 wt.% stock solution of gelatin (maintained at 50°C to prevent premature gelation) with water and acid. 1.5 M sodium citrate solution is prepared by dissolving sodium citrate tribasic dihydrate powder in deionized water by vigorously stirring.

The freeze-thawing step was completed by casting PVA precursor solution into petri dishes, which were frozen at −20°C for 5 h. The frozen solution was then brought to room temperature to thaw for approximately 15 min until all ice crystals disappeared to complete one freeze-thaw cycle. The freeze-thaw cycle was repeated four times unless otherwise noted, after which the precursor solution gelated into a mechanically weak PVA-FT hydrogel. Last, the salting-out step was done by immersing the PVA-FT gel in 1.5 M sodium citrate solution for 72 h to obtain a strong and tough PVA-SO hydrogel. Gelatin hydrogel was prepared using the same procedure using gelatin precursor solution.

To fabricate the PVA hydrogel via directional freezing, a precursor solution is injected into an acrylic mold that is thermally insulated on the sides using insulation tape and thermally conductive on a glass bottom. The container was lowered into a −80°C ethanol cooling bath (PSL1810, EYELA) at an immersion rate of 1 mm min^{-1}. The directionally frozen PVA solution was soaked in a 1.5 M sodium salt solution for 72 h to complete the salting-out process.

4.3 | Potentiometric Titration of Acidified PVA Solution

25 g 1HCl-PVA solution with a PVA concentration of 10 wt.% was prepared as described above. The solution had a density of 1.05 g cm^{-3}, translating to a total volume of 23.8 mL and an acid concentration of 1.05 M. An HCl solution with the same volume and concentration was used as a control. The 1HCl-PVA and HCl solution was titrated against 1 M NaOH, and the pH variation against NaOH volume was recorded using a pH meter (FiveEasy Plus pH meter, Mettler Toledo).

4.4 | Mechanical Testing

For tensile testing, hydrogels were cut into dog-bone shaped specimens with a gauge width of 1.5 mm. The thickness and width of each specimen were measured with a caliper. The stress–strain data were obtained using a mechanical tester (Univert, Cellscale). The specimens were stretched at a strain rate of 7.5% s^{-1}. The cyclic tensile test was conducted with the rectangular-shaped sample with a gauge width of 1.5 mm. The thickness and width of each specimen were measured with a caliper. The loading and unloading strain rates were both 7.5% s^{-1}. The sample was soaked in a salt solution bath during the whole test.

For compression testing, hydrogels were cut into circular specimens with a diameter of approximately 15 mm. The stress-strain data were obtained using a dynamic mechanical analyzer (DMA850, TA Instruments). The specimens were compressed at a strain rate of 8% min^{-1}.

4.5 | SEM Characterization

All hydrogel samples were immersed in DI water for 24 h to remove the salt from the gels. Afterward, the gel was frozen by liquid nitrogen and cracked by a rubber hammer to create un-damaged cross-sections. The samples were then freeze-dried using a freeze dryer (FreeZone, Labconco). The freeze-dried hydrogels were sputtered with gold with cross-sections upward before carrying out the imaging using SEM (Supra 40VP, ZEISS).

4.6 | UV–vis Spectroscopy

Hydrogels after the salting-out process were cut into samples of approximately 0.5 × 2 cm and placed into polystyrene cuvettes filled with 1.5 M sodium citrate solution to prevent dehydration and precipitation of salt crystals. The UV–vis spectra of the samples immersed in the sodium citrate solution were measured

using a spectrophotometer (UV-3101 PC, Shimadzu), with salt solution of the same concentration used as a reference.

4.7 | Mercury Intrusion Porosimetry

After salting-out, all hydrogel samples were immersed in DI water for 24 h to remove the salt followed by freeze drying. Pore size distribution and porosity of the dried samples were measured using a mercury intrusion porosimeter (PoreMaster 33, Anton Paar) in the intrusion mode under the pressure range of 0.0015 to 231 MPa.

4.8 | Differential Scanning Calorimetry

The crystallinities of hydrogels were measured using a differential scanning calorimeter (DSC250, TA Instruments). Prior to the DSC measurements, the amorphous parts of the hydrogels were crosslinked and fixed using glutaraldehyde. The samples were soaked in a solution consisting of glutaraldehyde (50 wt.%), HCl, and water (volume ratio of glutaraldehyde: HCl: water = 10:1:60). Then, the samples were immersed in a large amount of DI water for 24 h to remove the unreacted glutaraldehyde and hydrochloric acid. The samples were further freeze-dried and measured with DSC. The samples were weighed and heated from 50 to 250°C at a ramp rate of 20°C min^{-1}. The heat flow curve would show an endothermic peak between 200°C and 250°C that corresponds to the melting of PVA crystalline domains. Integration of this endothermic peak gives the enthalpy of melting of crystalline domains (H_c). The crystallinity can be calculated as $X_c = H_c / H_c^0$, where $H_c^0 = 138.6$ J g^{-1} is the enthalpy of the fusion of 100 wt.% crystalline PVA measured at the equilibrium melting point, T_m^0.

4.9 | Fatigue Tests

The single-notch method was used to measure the fatigue resistance of hydrogels. Fatigue testing was conducted in a bath of 1.5 M sodium citrate solution. The notched samples had an initial crack length (c_0) smaller than 1/5 of the width (L_0) of the sample. The cyclic stress–strain curves were measured using a mechanical tester (Univert, Cellscale). The energy release rate (G) was calculated using $G = 2kcW$, where k was empirically determined to be $k = 3/\sqrt{\varepsilon + 1}$, c was the crack length and W was the strain energy density of an unnotched sample with the same dimensions and stretched to the same strain. W was integrated from the loading curve of the unnotched sample after 250 cycles when the stress–strain curve became stable.

4.10 | Synthesis of PVAMA

To synthesize the methacrylate derivative of PVA, 20 g of PVA and 40 mg of hydroquinone were dissolved in 180 mL of DI at −20°C, followed by cooling to room temperature and addition of 10 mL methacrylic acid and 10 mL HCl. The reaction proceeded at 60°C for 24 h, which was then neutralized with 15 mL of triethylamine. The solution was diluted with 10 times DI water and added dropwise to acetone to precipitate the PVAMA. The precipitate was further washed with acetone and filtered, before drying under vacuum to remove the residual solvents.

4.11 | NMR Characterization

^{1}H NMR analysis was performed using a 400 MHz Bruker AV400 spectrometer. Precursor samples with various acidification ratios were prepared by mixing 0.2 g corresponding precursor with 1 mL D_2O.

4.12 | Fluorescence Lifetime Imaging Microscopy (FLIM)

FLIM imaging was performed with a Leica TCS-SP8-MP Imaging System in a phasor plotting approach. The experiment was conducted with a two-photon laser light source at 780 nm. The samples were prepared in the same procedure but use a precursor with 0.5 wt.% chromophore which was synthesized according to the reported method [92]. During the imaging, the samples were sandwiched between two slides of cover glass and sealed to prevent water evaporation.

4.13 | DLP Printing of PVAMA Hydrogels

The precursor used for printing consists of 3 wt.% PVA, 7 wt.% PVAMA, 0.1 wt.% TPO-Li, and 1 mol kg^{-1} HCl dissolved in water. The home-made printer was fabricated using a DLP-based PRO4500 UV light (385 nm) projector manufactured by Wintech Digital System Technology Corporation, a Thorlabs, Inc motorized translation stage, and optical accessories from Thorlabs, Inc. The power density of the projected UV light on the focal plane was measured to be 2.34 mW cm^{-2} using an ultraviolet light meter. A top-down configuration was used for DLP printing.

4.14 | Water Content Measurement

The hydrogels were immersed in water for 24 h to remove the acid and salt, before they were freeze-dried using a freeze dryer (FreeZone, Labconco). The weight before (m_w) and after (m_d) freeze drying was recorded, and the water content was calculated as $(m_w - m_d)/m_w \times 100\%$.

Acknowledgements

The authors acknowledge the support from American Chemical Society for award 66747-ND7, Johnson & Johnson for award 20231448, NIH for award R01DK132319, the Moore Foundation Award 12072, Semiconductor Research Corporation for award 2023-JU3136, and the Office of Naval Research (ONR) for awards N000142412187 and N000142212595.

Conflicts of Interest

The authors declare no conflict of interest.

Data Availability Statement

The data that support the findings of this study are available in the supplementary material of this article.;

References

1. K. Y. Lee and D. J. Mooney, "Hydrogels for Tissue Engineering," *Chemical Reviews* 101 (2001): 1869–1880, https://doi.org/10.1021/cr000108x.

2. J. Li and D. J. Mooney, "Designing Hydrogels for Controlled Drug Delivery," *Nature Reviews Materials* 1 (2016): 1–17.

3. Y. Zhao, C. Xuan, X. Qian, et al., "Soft Phototactic Swimmer Based on Self-Sustained Hydrogel Oscillator," *Science Robotics* 4 (2019): aax7112, https://doi.org/10.1126/scirobotics.aax7112.

4. N. Park and J. Kim, "Hydrogel-Based Artificial Muscles: Overview and Recent Progress," *Advanced Intelligent Systems* 2 (2020): 1900135.

5. J. L. Drury and D. J. Mooney, "Hydrogels for Tissue Engineering: Scaffold Design Variables and Applications," *Biomaterials* 24 (2003): 4337–4351, https://doi.org/10.1016/S0142-9612(03)00340-5.

6. H. Yuk, B. Lu, and X. Zhao, "Hydrogel Bioelectronics," *Chemical Society Reviews* 48 (2019): 1642–1667, https://doi.org/10.1039/C8CS00595H.

7. J.-Y. Sun, X. Zhao, W. R. K. Illeperuma, et al., "Highly Stretchable and Tough Hydrogels," *Nature* 489 (2012): 133–136, https://doi.org/10.1038/nature11409.

8. S. Lin, J. Liu, X. Liu, and X. Zhao, "Muscle-Like Fatigue-Resistant Hydrogels by Mechanical Training," *Proceedings of the National Academy of Sciences* 116 (2019): 10244–10249, https://doi.org/10.1073/pnas.1903019116.

9. I. Dellatolas, M. Bantawa, B. Damerau, et al., "Local Mechanism Governs Global Reinforcement of Nanofiller-Hydrogel Composites," *ACS Nano* 17 (2023): 20939–20948, https://doi.org/10.1021/acsnano.3c00716.

10. M. D. J. Hossen, S. D. Sarkar, M. M. Uddin, C. K. Roy, and M. S. Azam, "Mussel-Inspired Adhesive Nano-Filler for Strengthening Polyacrylamide Hydrogel," *ChemistrySelect* 5 (2020): 8906–8914.

11. X. Sun, Y. Mao, Z. Yu, P. Yang, and F. Jiang, "A Biomimetic "Salting Out—Alignment—Locking" Tactic to Design Strong and Tough Hydrogel," *Advanced Materials* 36 (2024): 2400084, https://doi.org/10.1002/adma.202400084.

12. X. Wang, S. Zheng, J. Xiong, et al., "Stretch-Induced Conductivity Enhancement in Highly Conductive and Tough Hydrogels," *Advanced Materials* 36 (2024): 2313845, https://doi.org/10.1002/adma.202313845.

13. M. Hua, S. Wu, Y. Ma, et al., "Strong Tough Hydrogels via the Synergy of Freeze-Casting and Salting Out," *Nature* 590 (2021): 594–599, https://doi.org/10.1038/s41586-021-03212-z.

14. X. He, D. Liu, B. Cui, et al., "Extreme Hydrogel Bioelectronics," *Advanced Functional Materials* 34 (2024): 2405896, https://doi.org/10.1002/adfm.202405896.

15. Y. Yan, S. Duan, B. Liu, et al., "Tough Hydrogel Electrolytes for Anti-Freezing Zinc-Ion Batteries," *Advanced Materials* 35 (2023): 2211673, https://doi.org/10.1002/adma.202211673.

16. M. Liu, X. Zeng, C. Ma, et al., "Injectable Hydrogels for Cartilage and Bone Tissue Engineering," *Bone Research* 5 (2017): 17014, https://doi.org/10.1038/boneres.2017.14.

17. S. Wang, Y. Chen, Y. Sun, et al., "Stretchable Slide-Ring Supramolecular Hydrogel For Flexible Electronic Devices," *Communications Materials* 3 (2022): 2.

18. Y. Zhang and P. S. Cremer, "Interactions Between Macromolecules and Ions: The Hofmeister Series," *Current Opinion in Chemical Biology* 10 (2006): 658–663, https://doi.org/10.1016/j.cbpa.2006.09.020.

19. S. Wu, M. Hua, Y. Alsaid, et al., "Poly(vinyl alcohol) Hydrogels With Broad-Range Tunable Mechanical Properties via the Hofmeister Effect," *Advanced Materials* 33 (2021): 2007829, https://doi.org/10.1002/adma.202007829.

20. X. Li and J. P. Gong, "Design Principles for Strong and Tough Hydrogels," *Nature Reviews Materials* 9 (2024): 380–398, https://doi.org/10.1038/s41578-024-00672-3.

21. L. Shu, X.-F. Zhang, Z. Wang, and J. Yao, "Structure Reorganization of Cellulose Hydrogel by Green Solvent Exchange for Potential Plastic Replacement," *Carbohydrate Polymers* 275 (2022): 118695, https://doi.org/10.1016/j.carbpol.2021.118695.

22. J. Huang, J. Liao, T. Wang, W. Sun, and Z. Tong, "Super Strong Dopamine Hydrogels With Shape Memory and Bioinspired Actuating Behaviours Modulated by Solvent Exchange," *Soft Matter* 14 (2018): 2500–2507, https://doi.org/10.1039/C8SM00297E.

23. T. Sakai, T. Matsunaga, Y. Yamamoto, et al., "Design and Fabrication of a High-Strength Hydrogel With Ideally Homogeneous Network Structure From Tetrahedron-Like Macromonomers," *Macromolecules* 41 (2008): 5379–5384, https://doi.org/10.1021/ma800476x.

24. M. Shibayama, X. Li, and T. Sakai, "Precision Polymer Network Science With Tetra-PEG Gels—A Decade History and Future," *Colloid and Polymer Science* 297 (2019): 1–12, https://doi.org/10.1007/s00396-018-4423-7.

25. L. Xu, S. Gao, Q. Guo, C. Wang, Y. Qiao, and D. Qiu, "A Solvent-Exchange Strategy to Regulate Noncovalent Interactions for Strong and Antiswelling Hydrogels," *Advanced Materials* 32 (2020): 2004579, https://doi.org/10.1002/adma.202004579.

26. S. Ladet, L. David, and A. Domard, "Multi-Membrane Hydrogels," *Nature* 452 (2008): 76–79, https://doi.org/10.1038/nature06619.

27. Y. Yang, X. Wang, F. Yang, H. Shen, and D. Wu, "A Universal Soaking Strategy to Convert Composite Hydrogels Into Extremely Tough and Rapidly Recoverable Double-Network Hydrogels," *Advanced Materials* 28 (2016): 7178–7184, https://doi.org/10.1002/adma.201601742.

28. L. Huang, H. Li, S. Wen, et al., "Control Nucleation for Strong and Tough Crystalline Hydrogels With High Water Content," *Nature Communications* 15 (2024): 7777, https://doi.org/10.1038/s41467-024-52264-y.

29. W. K. Son, J. H. Youk, T. S. Lee, and W. H. Park, "Effect of pH on Electrospinning of Poly(Vinyl Alcohol)," *Materials Letters* 59 (2005): 1571–1575, https://doi.org/10.1016/j.matlet.2005.01.025.

30. D. W. Smith, "Ionic Hydration Enthalpies," *Journal of Chemical Education* 54 (1977): 540, https://doi.org/10.1021/ed054p540.

31. J. P. Gong, Y. Katsuyama, T. Kurokawa, and Y. Osada, "Double-Network Hydrogels With Extremely High Mechanical Strength," *Advanced Materials* 15 (2003): 1155–1158, https://doi.org/10.1002/adma.200304907.

32. J. Fang, A. Mehlich, N. Koga, et al., "Forced Protein Unfolding Leads to Highly Elastic and Tough Protein Hydrogels," *Nature Communications* 4 (2013): 2974, https://doi.org/10.1038/ncomms3974.

33. W. R. K. Illeperuma, J.-Y. Sun, Z. Suo, and J. J. Vlassak, "Fiber-Reinforced Tough Hydrogels," *Extreme Mechanics Letters* 1 (2014): 90–96, https://doi.org/10.1016/j.eml.2014.11.001.

34. Q. Chen, L. Zhu, H. Chen, et al., "A Novel Design Strategy for Fully Physically Linked Double Network Hydrogels With Tough, Fatigue Resistant, and Self-Healing Properties," *Advanced Functional Materials* 25 (2015): 1598–1607, https://doi.org/10.1002/adfm.201404357.

35. P. Lin, S. Ma, X. Wang, and F. Zhou, "Molecularly Engineered Dual-Crosslinked Hydrogel With Ultrahigh Mechanical Strength, Toughness, and Good Self-Recovery," *Advanced Materials* 27 (2015): 2054–2059, https://doi.org/10.1002/adma.201405022.

36. F. Luo, T. L. Sun, T. Nakajima, et al., "Oppositely Charged Polyelectrolytes Form Tough, Self-Healing, and Rebuildable Hydrogels," *Advanced Materials* 27 (2015): 2722–2727.

37. X. Hu, M. Vatankhah-Varnoosfaderani, J. Zhou, Q. Li, and S. S. Sheiko, "Weak Hydrogen Bonding Enables Hard, Strong, Tough, and Elastic Hydrogels," *Advanced Materials* 27 (2015): 6899–6905, https://doi.org/10.1002/adma.201503724.

38. P. Lin, T. Zhang, X. Wang, B. Yu, and F. Zhou, "Freezing Molecular Orientation Under Stretch for High Mechanical Strength but Anisotropic Hydrogels," *Small* 12 (2016): 4386–4392.

39. D. Xu, J. Huang, D. Zhao, B. Ding, L. Zhang, and J. Cai, "High-Flexibility, High-Toughness Double-Cross-Linked Chitin Hydrogels by Sequential Chemical and Physical Cross-Linkings," *Advanced Materials* 28 (2016): 5844–5849, https://doi.org/10.1002/adma.201600448.

40. D. Zhao, J. Huang, Y. Zhong, K. Li, L. Zhang, and J. Cai, "High-Strength and High-Toughness Double-Cross-Linked Cellulose Hydrogels: A New Strategy Using Sequential Chemical and Physical Cross-Linking," *Advanced Functional Materials* 26 (2016): 6279–6287, https://doi.org/10.1002/adfm.201601645.

41. B. Xu, P. Zheng, F. Gao, et al., "A Mineralized High Strength and Tough Hydrogel for Skull Bone Regeneration," *Advanced Functional Materials* 27 (2017): 1604327, https://doi.org/10.1002/adfm.201604327.

42. M. T. I. Mredha, Y. Z. Guo, T. Nonoyama, T. Nakajima, T. Kurokawa, and J. P. Gong, "A Facile Method to Fabricate Anisotropic Hydrogels With Perfectly Aligned Hierarchical Fibrous Structures," *Advanced Materials* 30 (2018): 1704937, https://doi.org/10.1002/adma.201704937.

43. Q. He, Y. Huang, and S. Wang, "Hofmeister Effect-Assisted One Step Fabrication of Ductile and Strong Gelatin Hydrogels," *Advanced Functional Materials* 28 (2018): 1705069, https://doi.org/10.1002/adfm.201705069.

44. K. Voges, C. Hübner, M. Vadalá, and D. C. Lupascu, "Ice-Templated Poly(vinyl alcohol): Enhanced Strength and Low Thermal Conductivity," *Macromolecular Materials and Engineering* 303 (2018): 1800198, https://doi.org/10.1002/mame.201800198.

45. M. T. I. Mredha, H. H. Le, V. T. Tran, P. Trtik, J. Cui, and I. Jeon, "Anisotropic Tough Multilayer Hydrogels With Programmable Orientation," *Material Horizons* 6 (2019): 1504–1511.

46. S. Lin, X. Liu, J. Liu, et al., "Anti-Fatigue-Fracture Hydrogels," *Science Advances* 5 (2019): aau8528, https://doi.org/10.1126/sciadv.aau8528.

47. X. Li, K. Cui, T. L. Sun, et al., "Mesoscale Bicontinuous Networks in Self-Healing Hydrogels Delay Fatigue Fracture," *Proceedings of the National Academy of Sciences* 117 (2020): 7606–7612.

48. Y. Bai, J. Zhang, D. Wen, et al., "Fabrication of Remote Controllable Devices With Multistage Responsiveness Based on a NIR Light-Induced Shape Memory Ionomer Containing Various Bridge Ions," *Journal of Materials Chemistry A* 7 (2019): 20723–20732, https://doi.org/10.1039/C9TA05329H.

49. W. Chen, D. Li, Y. Bu, G. Chen, X. Wan, and N. Li, "Design of Strong and Tough Methylcellulose-Based Hydrogels Using Kosmotropic Hofmeister Salts," *Cellulose* 27 (2020): 1113–1126, https://doi.org/10.1007/s10570-019-02871-6.

50. S. Gupta, S. Goswami, and A. Sinha, "A Combined Effect of Freeze–Thaw Cycles and Polymer Concentration on the Structure and Mechanical Properties of Transparent PVA Gels," *Biomedical Materials* 7 (2012): 015006.

51. Y. Liu, N. E. Vrana, P. A. Cahill, and G. B. McGuinness, "Physically Crosslinked Composite Hydrogels of PVA With Natural Macromolecules: Structure, Mechanical Properties, and Endothelial Cell Compatibility," *Journal of Biomedical Materials Research Part B: Applied Biomaterials* 90B (2009): 492–502, https://doi.org/10.1002/jbm.b.31310.

52. L. Xie, M. Jiang, X. Dong, X. Bai, J. Tong, and J. Zhou, "Controlled Mechanical and Swelling Properties of Poly(Vinyl Alcohol)/Sodium Alginate Blend Hydrogels Prepared by Freeze–Thaw Followed by Ca^{2+} Crosslinking," *Journal of Applied Polymer Science* 124 (2012): 823–831, https://doi.org/10.1002/app.35083.

53. Y. Huang, M. Zhang, and W. Ruan, "High-Water-Content Graphene Oxide/Polyvinyl Alcohol Hydrogel With Excellent Mechanical Properties," *Journal of Materials Chemistry A* 2 (2014): 10508–10515, https://doi.org/10.1039/C4TA01464B.

54. Q. Zheng, A. Javadi, R. Sabo, Z. Cai, and S. Gong, "Polyvinyl Alcohol (PVA)–Cellulose Nanofibril (CNF)–Multiwalled Carbon Nanotube (MWCNT) Hybrid Organic Aerogels With Superior Mechanical Properties," *RSC Advances* 3 (2013): 20816–20823.

55. A. Javadi, Q. Zheng, F. Payen, et al., "Polyvinyl Alcohol-Cellulose Nanofibrils-Graphene Oxide Hybrid Organic Aerogels," *ACS Applied Materials & Interfaces* 5 (2013): 5969–5975, https://doi.org/10.1021/am400171y.

56. G. Nian, J. Kim, X. Bao, and Z. Suo, "Making Highly Elastic and Tough Hydrogels From Doughs," *Advanced Materials* 34 (2022): 2206577, https://doi.org/10.1002/adma.202206577.

57. Y. Wu, Y. Zhang, H. Wu, et al., "Solvent-Exchange-Assisted Wet Annealing: A New Strategy for Superstrong, Tough, Stretchable, and Anti-Fatigue Hydrogels," *Advanced Materials* 35 (2023): 2210624, https://doi.org/10.1002/adma.202210624.

58. C. Liu, N. Morimoto, L. Jiang, et al., "Tough Hydrogels With Rapid Self-Reinforcement," *Science* 372 (2021): 1078–1081, https://doi.org/10.1126/science.aaz6694.

59. Y. Xie, S. Gao, Z. Ling, et al., "A Multiscale Biomimetic Strategy to Design Strong, Tough Hydrogels by Tuning the Self-Assembly Behavior of Cellulose," *Journal of Materials Chemistry A* 10 (2022): 13685–13696, https://doi.org/10.1039/D2TA03262G.

60. W. Li, S. Zheng, X. Zou, et al., "Tough Hydrogels With Isotropic and Unprecedented Crack Propagation Resistance," *Advanced Functional Materials* 32 (2022): 2207348, https://doi.org/10.1002/adfm.202207348.

61. H. Fan, J. Wang, and J. P. Gong, "Barnacle Cement Proteins-Inspired Tough Hydrogels With Robust, Long-Lasting, and Repeatable Underwater Adhesion," *Advanced Functional Materials* 31 (2021): 2009334, https://doi.org/10.1002/adfm.202009334.

62. Y. Yang, Y. Yang, Y. Cao, et al., "Anti-Freezing, Resilient and Tough Hydrogels for Sensitive and Large-Range Strain and Pressure Sensors," *Chemical Engineering Journal* 403 (2021): 126431, https://doi.org/10.1016/j.cej.2020.126431.

63. M. Hua, S. Wu, Y. Jin, Y. Zhao, B. Yao, and X. He, "Tough-Hydrogel Reinforced Low-Tortuosity Conductive Networks for Stretchable and High-Performance Supercapacitors," *Advanced Materials* 33 (2021): 2100983, https://doi.org/10.1002/adma.202100983.

64. Q. Zhang, Q. Wang, G. Wang, Z. Zhang, S. Xia, and G. Gao, "Ultrathin and Highly Tough Hydrogel Films for Multifunctional Strain Sensors," *ACS Applied Materials & Interfaces* 13 (2021): 50411–50421, https://doi.org/10.1021/acsami.1c15784.

65. H. J. Zhang, T. L. Sun, A. K. Zhang, et al., "Tough Physical Double-Network Hydrogels Based on Amphiphilic Triblock Copolymers," *Advanced Materials* 28 (2016): 4884–4890, https://doi.org/10.1002/adma.201600466.

66. S. Han, Q. Wu, J. Zhu, et al., "Tough Hydrogel With High Water Content and Ordered Fibrous Structures as an Artificial Human Ligament," *Materials Horizons* 10 (2023): 1012–1019, https://doi.org/10.1039/D2MH01299E.

67. G. Zhang, J. Steck, J. Kim, C. H. Ahn, and Z. Suo, "Hydrogels of Arrested Phase Separation Simultaneously Achieve High Strength and Low Hysteresis," *Science Advances* 9 (2023): adh7742.

68. Y. Xu, J. Tan, W. Dong, et al., "Super Strong and Tough Hydrogels Constructed via Network Uniformization of Macromolecular Chains," *Advanced Functional Materials* 35 (2025): 2419161, https://doi.org/10.1002/adfm.202419161.

69. S. Wu, Z. Liu, C. Gong, et al., "Spider-Silk-Inspired Strong and Tough Hydrogel Fibers With Anti-Freezing And Water Retention Properties," *Nature Communications* 15 (2024): 4441, https://doi.org/10.1038/s41467-024-48745-9.

70. Y. Shi, B. Wu, S. Sun, and P. Wu, "Aqueous Spinning of Robust, Self-Healable, and Crack-Resistant Hydrogel Microfibers Enabled by Hydrogen Bond Nanoconfinement," *Nature Communications* 14 (2023): 1370, https://doi.org/10.1038/s41467-023-37036-4.

71. F. Hu, B. Dong, R. Zhao, et al., "Lignosulfonate Sodium and Ionic Liquid Synergistically Promote Tough Hydrogels for Intelligent Wearable Human-Machine Interaction," *International Journal of Biological*

Macromolecules 254 (2024): 127958, https://doi.org/10.1016/j.ijbiomac.2023.127958.

72. J. Deng, H. Liu, D. Liu, et al., "Room-Temperature Phosphorescent Tough Hydrogels Based on Ionically Crosslinked Nonaromatic Polymers," *Advanced Functional Materials* 34 (2024): 2308420, https://doi.org/10.1002/adfm.202308420.

73. S. Wang, Z. Yu, X. Sun, et al., "A Universal Strategy to Mitigate Microphase Separation via Cellulose Nanocrystal Hydration in Fabricating Strong, Tough, and Fatigue-Resistant Hydrogels," *Advanced Materials* 37 (2025): 2416916, https://doi.org/10.1002/adma.202416916.

74. S. Wang, L. Lei, Y. Tian, et al., "Strong, Tough and anisotropic bioinspired hydrogels," *Materials Horizons* 11 (2024): 2131–2142, https://doi.org/10.1039/D3MH02032K.

75. Z. Huang, Z. Wu, C. Li, et al., "Self-Healing Yet Strong Actuator Materials With Muscle-Like Diastole and Contraction via Multilevel Relaxations," *Advanced Materials* 37 (2025): 2413194, https://doi.org/10.1002/adma.202413194.

76. X. Yang, X. Huang, X. Qiu, Q. Guo, and X. Zhang, "Supramolecular Metallic Foams With Ultrahigh Specific Strength and Sustainable Recyclability," *Nature Communications* 15 (2024): 4553, https://doi.org/10.1038/s41467-024-49091-6.

77. X. Yao, S. Zhang, N. Wei, et al., "Poly (Ionic Liquid) Functionalization: A General Strategy for Strong, Tough, Ionic Conductive, and Multifunctional Polysaccharide Hydrogels Toward Sensors," *SusMat* 4 (2024): 249.

78. M. V. Fedkin, Y. K. Shin, N. Dasgupta, et al., "Development of the ReaxFF Methodology for Electrolyte–Water Systems," *The Journal of Physical Chemistry A* 123 (2019): 2125–2141, https://doi.org/10.1021/acs.jpca.8b10453.

79. S. Monti, A. Corozzi, P. Fristrup, et al., "Exploring the Conformational And Reactive Dynamics Of Biomolecules In Solution Using An Extended Version Of The Glycine Reactive Force Field," *Physical Chemistry Chemical Physics* 15 (2013): 15062–15077, https://doi.org/10.1039/c3cp51931g.

80. K. Chenoweth, A. C. T. van Duin, and W. A. Goddard, "ReaxFF Reactive Force Field for Molecular Dynamics Simulations of Hydrocarbon Oxidation," *The Journal of Physical Chemistry A* 112 (2008): 1040–1053, https://doi.org/10.1021/jp709896w.

81. A. D. Bochevarov, E. Harder, T. F. Hughes, et al., "Jaguar: A High-Performance Quantum Chemistry Software Program With Strengths in Life and Materials Sciences," *International Journal of Quantum Chemistry* 113 (2013): 2110–2142, https://doi.org/10.1002/qua.24481.

82. A. Michele, P. Paschkowski, C. Hänel, G. E. M. Tovar, T. Schiestel, and A. Southan, "Acid Catalyzed Cross-Linking of Polyvinyl Alcohol for Humidifier Membranes," *Journal of Applied Polymer Science* 139 (2022): 51606, https://doi.org/10.1002/app.51606.

83. E. Rynkowska, K. Fatyeyeva, S. Marais, J. Kujawa, and W. Kujawski, "Chemically and Thermally Crosslinked PVA-Based Membranes: Effect on Swelling and Transport Behavior," *Polymers* 11 (2019): 1799, https://doi.org/10.3390/polym11111799.

84. S. D. Desai, I. Kundu, N. P. Swamy, et al., "Cross-Linking of Poly (Vinyl Alcohol) Films Under Acidic And Thermal Stress," *European Journal of Pharmaceutical Sciences* 152 (2020): 105429, https://doi.org/10.1016/j.ejps.2020.105429.

85. F. Ni, P. Xiao, C. Zhang, and T. Chen, "Hygroscopic Polymer Gels Toward Atmospheric Moisture Exploitations for Energy Management and Freshwater Generation," *Matter* 5 (2022): 2624–2658.

86. Y. Liu, S. Shen, Z. Duan, J. Deng, and D. Fan, "Hydrogels for Long-Term Moisture Retention Under Ambient Conditions: Inhibiting the Evaporation of Free Water From Macroscopic to Molecular Scales," *Advanced Functional Materials* 35 (2025): 2504356, https://doi.org/10.1002/adfm.202504356.

87. H. Yuk, T. Zhang, G. A. Parada, X. Liu, and X. Zhao, "Skin-Inspired Hydrogel–Elastomer Hybrids With Robust Interfaces and Functional Microstructures," *Nature Communications* 7 (2016): 12028, https://doi.org/10.1038/ncomms12028.

88. Y. Huang, T. Zhu, H. Yuan, et al., "An in Situ Encapsulation Strategy for Enhancing the Stability of Hydrogels in Both Air and Water Through Surface-Confined Copolymerization," *Chemical Engineering Journal* 485 (2024): 149847, https://doi.org/10.1016/j.cej.2024.149847.

89. H. Yuan, T. Zhu, Y. Huang, et al., "Hydrophobic and Adhesive Elastomer Encapsulation for Anti-Drying, Non-Swelling, and Adhesive Hydrogels," *Advanced Functional Materials* 34 (2024): 2409703, https://doi.org/10.1002/adfm.202409703.

90. S. Sakurai, T. Kurokawa, H. Furukawa, J. P. Gong, and T. Nakajima, "Double-Network Hydrogels With a Gradient Hydrophobic Coating that Prevents Water Evaporation and Allows Strong Adhesion to a Solid Substrate," *Polymer Journal* 57 (2025): 441–447, https://doi.org/10.1038/s41428-024-01010-8.

91. Y. Li, C. Ni, R. Cao, et al., "Sprayable Porous Hydrogel Coating for Efficient and Sustainable Evaporative Cooling," *Matter* 7 (2024): 4270–4280.

92. Y. Yu, M. Si, W. Lu, et al., "Confining Monochromophore in Dynamic Polymer Network for Multi-Stimuli Responsive Fluorescence-Phosphorescence Dual-Emission," *Chemical Engineering Journal* 478 (2023): 147271, https://doi.org/10.1016/j.cej.2023.147271.

Supporting Information

Additional supporting information can be found online in the Supporting Information section.

Supporting File: adma72542-sup-0001-SuppMat.docx.